

Real-time pupil tracking backlight system for holographic 3D display

(Invited Paper)

Hyon-Gon Choo¹, Minsik Park¹, Hyun-Eui Kim¹, Chanyeol Bae²,
Byung Gyu Chae¹, Hwi Kim², Kyungae Moon¹, Jinwoong Kim¹,
and Joonku Hahn^{3*}

¹Electronics and Telecommunications Research Institute, Taejon 305-700, Korea

²Korea University, Sejong Campus, Sejong 339-700, Korea

³Kyungpook National University, Daegu 702-701, Korea

*Corresponding author: jhahn@knu.ac.kr

Received February 27, 2014; accepted April 4, 2014; posted online May 28, 2014

We propose an automatic three-dimensional (3D) pupil tracking backlight system for holographic 3D display system with large image size and full-parallax accommodation effect. The proposed tracking module is applied to a holographic 3D display system with two sets of directional holographic imaging module composed of 2×2 large scale lens array and 22-inch high-resolution liquid crystal display 3D panel. System architecture is described and experimental results are presented.

OCIS codes: 090.2870, 090.1705, 090.1760.

doi: 10.3788/COL201412.060004.

Holographic three-dimensional (3D) displays have been actively researched for generating realistic 3D images in free space for last decades. The spatial light modulator (SLM) technology for control and manipulation of wave front of light wave in free space is a core technology for the holographic 3D imaging. In practice, however, commercially available SLMs have technological limitation in pixel size, screen size, and dynamic range for realistic holographic 3D display.

The information capacity of an SLM in holographic 3D display is theoretically represented by the space-bandwidth product^[1]. The space-bandwidth product is interpreted as the product of the holographic image size and viewing angle and its invariance means that there is a robust trade-off relationship between image size and viewing angle in any type of holographic 3D displays using SLM.

With respect to engineering viewpoint, there can be indirect methods for widening viewing angle by time-domain technique such as fast sequential scanning of holographic images or spatial domain technique such as optical spatial multiplexing of independent holographic display modules^[2-6].

We can take a strategy that large size image is, firstly, secured and then the viewing angle widening issue is resolved. The SeeReal have shown a holographic display system with the tracked viewing window (VW) technique^[7-11]. The directional backlight system synchronized with an eye-tracking module enables observer to see holographic image comfortably in a specified range of a VW plane. It is known that in the system of SeeReal, the observer's VW should be in a specified plane distant from the display system since the directional backlight system can control the focal point position only hor-

izontally, thus does not provide an adaptive focusing functionality along the axial direction. In addition, since vertical-only hologram patterns are used, their system cannot show full parallax accommodation effect.

In this letter, we propose an automatic 3D pupil tracking backlight system for holographic 3D display system with large image size and full-parallax accommodation effect. The pupil tracking system is composed of hybrid camera setup using Kinect and stereo camera and motorized XYZ stage for 3D pupil tracking. The proposed tracking module is applied to a holographic 3D display system. The display system provides large size stereoscopic holographic 3D images to a freely movable observer in a real-time manner through two sets of directional holographic imaging module composed of 2×2 large scale lens array and 22-inch high-resolution liquid crystal display (LCD) panel^[12].

In Fig. 1(a), the layout of one lens in the display system is illustrated. A diverging light emitted from a point light source is transformed to a spherical convergent wave toward a VW created in the focal plane of the field lens. The computer generated hologram (CGH) displayed in the SLM generates a holographic 3D scene to the observer through the narrow VW. The VW position can be changed according to the position of the point source. As shown in Figs. 1(b) and (c), if we can control the 3D position of the point source, the VW tracking range can be also a 3D volume.

The relation between the position of the VW and that of the light source can be derived from a simple geometric optics of the field lens. If the lens is assumed to be the first-order optical lens with an effective focal length f_{eff} , and (x_s, y_s, z_s) represents the relative position of a light source at the distance d_o from the front principal plane of the lens, the relative position of the VW, $(x_{vw},$

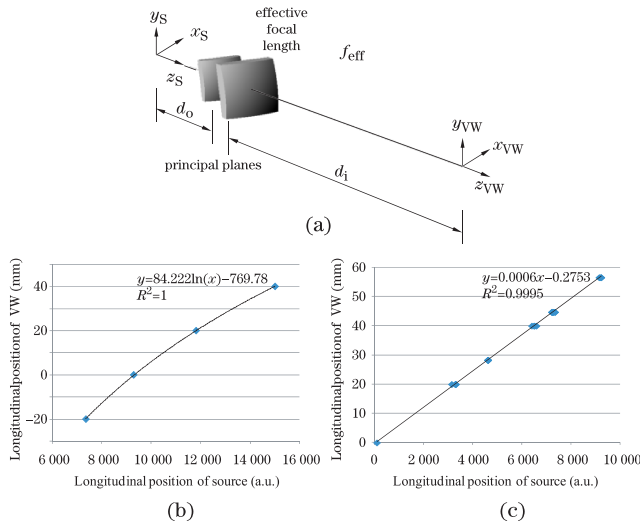


Fig. 1. (a) Positions of source and VW relations between two positions (b) along the longitudinal direction and (c) along the transverse direction.

y_{VW}, z_{VW}) at the distance d_i from the rear principal plane can be determined by

$$\frac{1}{z_{VW} + d_i} + \frac{1}{z_S + d_o} = \frac{1}{f_{eff}}. \quad (1)$$

From Eq. (1), the longitudinal position of VW is obtained as

$$\begin{aligned} z_{VW} &= \frac{f_{eff}(z_S + d_o)}{z_S + d_o - f_{eff}} - d_i \\ &\approx \frac{f_{eff}d_o}{z_S} - d_i. \end{aligned} \quad (2)$$

Here, the approximation is valid when the difference between effective focal length and the distance d_o is relatively small in comparison of the position of the source. This relation along the longitudinal direction is shown in Fig. 1(b) and the correlation coefficient of the regression is almost one. The relation along the transverse direction is shown in Fig. 1(c) and it is reasonable that the relation along the transverse direction is regarded as simply linear.

Let us denote the SLM pixel pitch, wavelength of light, and the distance between SLM and VW by p , λ , and d , respectively. The size of the VW can be obtained by

$$w = d\lambda/p. \quad (3)$$

For example, for 125- μm pixel pitch of the SLM, 2,600-mm focal length of the lens, and 532-nm wavelength (green laser light), the VW size is 11.06 mm. To adjust such a small VW of the display to the observer's pupil, precise pupil tracking is required. If we assume that the size of the human pupil is 6 mm, the error for pupil tracking should be less than 5 mm in order to place the observer's pupil inside the VW. Also for reliable watching, the pupil tracking should be performed in a real-time manner. The schematic diagram of our holographic display system is shown in Figs. 2(a) and (b). The display modules are designed to be optically multiplexed to deliver left and right stereoscopic holographic images to

observers as indicated in Fig. 2(c).

In our implementation, two 22-inch IBM T221 LCD panels with 3,840 \times 2,400 resolution are used for SLMs^[12]. The field lens is designed by the form of 2 \times 2 lens array with finely tuned tilted axial alignment as shown in Fig. 2(c). The optical transmittance of the lens array with tilting axes is optically equivalent to large diameter field lens. The rectangular aperture size of a unit lens is 144 \times 144 (mm), and a 2 \times 2 lens array composed of 4 unit lens covers 2,400 \times 2,400 square pixels in our system. Through each sub-lens system, the light starting from 0.5 m behind the lens system is designed to focus at the 2.6 m from the lens system. For each unit lens in the 2 \times 2 lens array backlight system, four independent white laser sources are installed. In this configuration, the position alignment of four laser sources is critical to make a converging field toward a single focal point. Furthermore, dynamic pupil tracking module is synchronized with the position control mechanics of the four light sources for precise 3D positional control of the VW in free space. Considering the aberration of the 2 \times 2 lens array, we set the effective observation area to the volume constraint from -100 to +100 mm in longitudinal direction and from -110 to +110 mm in transverse direction.

The light source produces white light by combining R/G/B laser sources. For easy alignment of the optical components, the fiber coupled laser is used for single color light source. The light wave from the white light source is split into two paths for left and right eyes. The end of a light source is connected to a collimating unit composed of a polarizer, a half wave plate and an objective lens. Each collimating unit is mounted on a motorized stage for changing direction of the light.

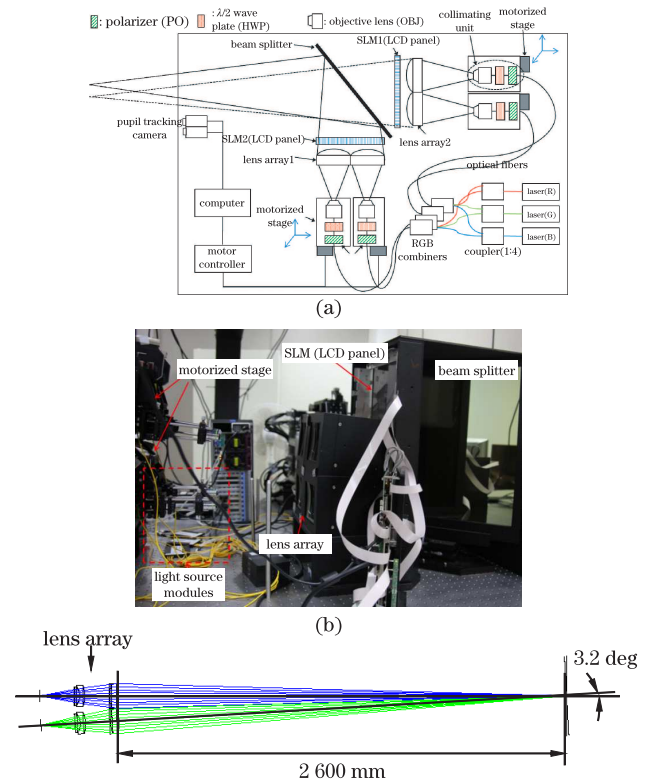


Fig. 2. (a) Schematic diagram and (b) implemented holographic 3D display setup, and (c) layout of the lens array.

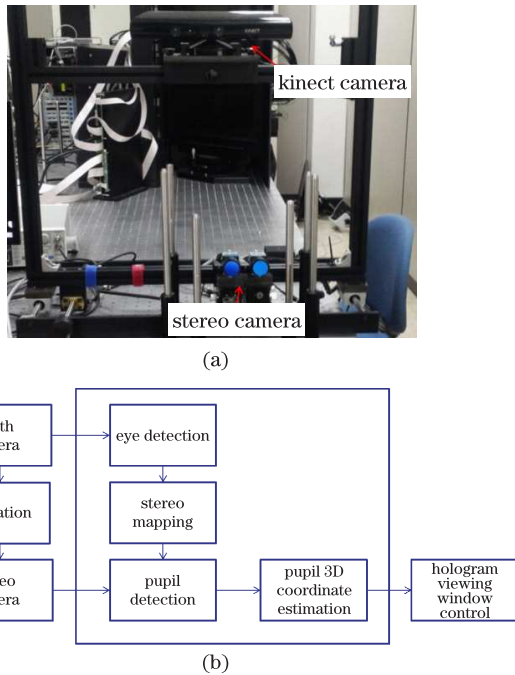


Fig. 3. (a) Pupil tracking system and (b) procedure in the pupil tracking system.

To support the holographic stereogram, two light waves from different optical paths are combined by a high quality half-mirror installed along the diagonal direction between two orthogonal display panels.

The proposed pupil tracking consists of Kinect and stereo-camera vision of which the pixel resolution is $1,600 \times 1,200$ as shown in Fig. 3(a). The pupil tracking camera system is located at 1 m distance from the observer to increase its spatial and depth resolution. In our approach, we utilize pupil tracking approach using hybrid camera composition of Kinect and stereo camera. Kinect camera provides face and eye tracking results itself^[13]. However, it does not provide enough accuracy for eye tracking due to its limited resolution. Thus, in our approach, the face and eye tracking results from Kinect are used for initial candidate selection, and 3D coordinates of the pupil is estimated using captured images from stereo camera with high resolution. Figure 3(b) shows the procedure of the pupil tracking method.

According to the procedure in Fig. 3(b), 3D eye coordinates are calculated in Kinect first, and translated into the two-dimensional (2D) pixel positions of the stereo camera. For this translation, the mapping matrix between Kinect 3D coordinates and the 2D pixel positions of the stereo camera is needed. This relationship is almost the same as the projection of the 3D world coordinate into 2D plane, and is represented as following:

$$\mathbf{x} = \mathbf{P}\mathbf{X}, \quad (4)$$

where \mathbf{P} is mapping matrix. $\mathbf{P} = \begin{pmatrix} p_{11} & p_{12} & p_{13} \\ p_{21} & p_{22} & p_{23} \end{pmatrix}$ transform 3D coordinate $\mathbf{X} = (X \ Y \ Z)^T$ of the Kinect camera to a 2D pixel position $\mathbf{x} = (x \ y)^T$ of a captured image from one of stereo cameras. The mapping matrix \mathbf{P} can be estimated by the following optimization problem

$$\min_{\mathbf{P}} \sum_i \| (x_i \ y_i)^T - \mathbf{P}(X_i \ Y_i \ Z_i)^T \|^2. \quad (5)$$

For eye position obtained by the matrix \mathbf{P} , we assume that the pupil should exist around the estimated eye position. For accurate pupil localization, we utilize the characteristics of pupil area regarding brightness and shape. The pupil is known to be one of the darkest areas around the eye and its shape is similar to a circle. From the prior knowledge, we first select the candidates using a threshold estimated from local minima. Then, among the candidates, the region with the highest circularity ratio is selected as the pupil region, and its center position is selected as that of the pupil. Compactness, the ratio of the area of the shape to the area of a circle having the same perimeter, is used as a measurement for circularity ratio. For a pupil, when 2D pixel positions from the stereo image are obtained, the 3D coordinate is calculated using camera parameters and pixel disparity, and the pupil center coordinate is transferred to the motorized stage controller in order to adjust the light source.

Figure 4 shows the experimental results of the pupil tracking. The detected eyes from Kinect (right-top image) and the extracted pupils from stereo camera (left-top image) are shown. The left-bottom and right-bottom images in Fig. 4 represent the mapping results from eye

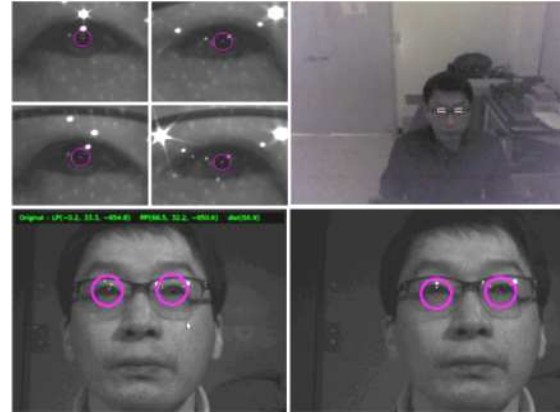


Fig. 4. Pupil tracking and VW formation.

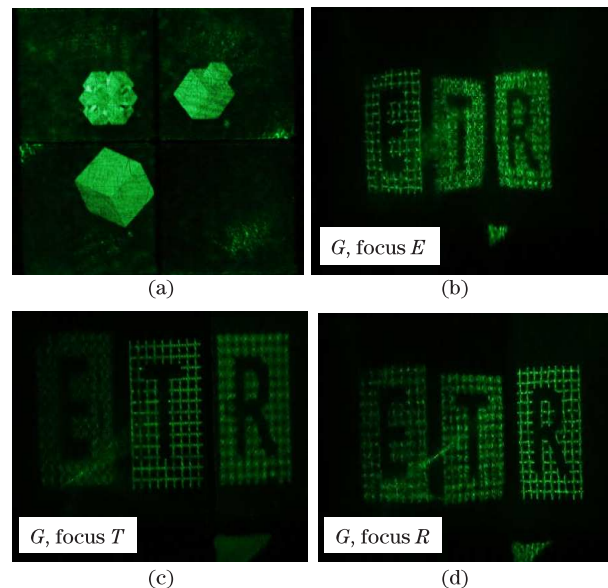


Fig. 5. Experimentally captured images.

position of the Kinect camera to 2D stereo vision. The experimental result showed that our method can successfully extract pupil position and adjust the VW of the display into the observer's pupil accurately.

In Fig. 5, the reconstruction results of mono-color holographic 3D images are presented. The CGH is synthesized using the classical off-axis amplitude encoding of depth-map 3D object CGH and polygon CGH^[14]. In Figures 5(a), exemplary experimental reconstruction result of mono-color polygon CGH images captured by our display system is presented. Figs. 5(b), (c), and (d) are the depth-map holographic images demonstrating the full-parallax accommodation effect.

In conclusion, we propose the automatic 3D pupil tracking backlight system for holographic 3D display system with large image size and full-parallax accommodation effect. In the proposed system, the movable light source on motorized stages and the pupil tracking system is interlocked. For the future work, we will try to implement a holographic 3D display system using electrically steerable pupil tracking backlight system with simpler and slimmer structure.

This work was supported by GigaKOREA project (GK13D0100, Development of Telecommunications Terminal with Digital Holographic Table-top Display).

References

1. A. W. Lohmann, R. G. Dorsch, D. Mendlovic, Z. Zalevsky, and C. Ferreira, *J. Opt. Soc. Am. A* **13**, 470 (1996).
2. J. Hahn, H. Kim, Y. Lim, G. Park, and B. Lee, *Opt. Express* **16**, 12372 (2008).
3. L. Onural, F. Yaraz, and H. Kang, *Proc. IEEE* **99**, 576 (2011).
4. T. Kozacki, G. Finke, P. Garbat, W. Zaperty, and M. Kujawińska, *Opt. Express* **20**, 27473 (2012).
5. M. Stanley, M. A. Smith, A. P. Smith, P. J. Watson, S. D. Coomber, C. D. Cameron, C. W. Slinger, and A. Wood, *Proc. SPIE* **5249**, 297 (2003).
6. Y. Takaki and N. Okada, *Appl. Opt.* **48**, 3255 (2009).
7. R. Haussler, A. Schwerdtner, and N. Leister, *Proc. SPIE* **6803**, 68030M (2008).
8. S. Reichelt, R. Haussler, N. Leister, G. Fütterer, H. Stolle, and A. Schwerdtner, in *Advances in Lasers and Electro Optics*, N. Costa and A. Cartaxo (eds.) (InTech, 2010) chap. 29.
9. Zschau, Enrico, and S. Reichelt, in *Handbook of Visual Display Technology*, J. Chen, W. Cranton, and M. Fihn (eds.) (Springer, Berlin Heidelberg, 2012) pp. 1875-1897.
10. S. Reichelt, R. Häussler, G. Fütterer, N. Leister, H. Kato, N. Usukura, and Y. Kanbayashi, *Opt. Lett.* **37**, 1955 (2012).
11. S. Reichelt and N. Leister, *J. Phys.: Conf. Ser.* **415**, 012038 (2013).
12. Minsik Park, Byung Gyu Chae, Hyun-Eui kim, Joonku Hahn, Hwi kim, Cheong Hee Park, Kyungae Moon, and Jinwoong kim, *ETRI Journal* **36**, 232 (2014).
13. *Kinect for Windows*, <http://www.microsoft.com/en-us/kinectforwindows/>.
14. H. Kim, J. Hahn, and B. Lee, *Appl. Opt.* **47**, D117 (2008).